Activity report on the project "*Evaluating photodegradation products of plastic nurdles and their toxicity in Matagorda Bay*"

PIs: Zhanfei Liu, The University of Texas at Austin; Wei Xu, Texas A&M University Corpus Christi

Period: June 1st, 2024, to October 30st, 2024

Part I. **Tracking the photooxidation products of primary plastic pellets (nurdles) in the marine environment**

Abstract

Marine plastic debris often undergoes photooxidation through sunlight exposure, potentially releasing substances that impact ecosystem health and carbon cycling. However, the photochemical modification of plastic polymers remains poorly understood. In this study, we investigated photooxidation dynamics of two common plastic types—polyethylene (PE) and polycarbonate (PC) nurdles through 8-week laboratory simulations, representing 1.5 years of natural sunlight exposure along the Texas coast. Through Fourier-transform infrared spectroscopy (FTIR), we observed surface oxidation on the nurdles, with the incorporation of oxygen into the plastic chains as carbonyl and carboxyl groups. This exposure also facilitated the leaching of dissolved organic carbon (DOC) to seawater, with PE pellets releasing significantly more DOC than PC pellets—by an 18-fold difference, likely due to differences in polymer properties and oxygen availability. No nano-sized plastic particles were detected after ultrafiltration (3k Da cut-off) and microscopic scanning. High-resolution mass spectrometry analysis further revealed that sunlight exposure increased the number of molecular formulas in the plastic-derived DOC, with their stoichiometry reflecting the polymers' chemical compositions. Additionally, the oxygen-to-carbon ratio in PE-derived DOC increased over time, while the hydrogen-to-carbon ratio in PC-derived DOC

decreased, indicating an enrichment of oxygenated compounds, likely due to an increase in carboxyl groups on nurdle surface during later stages of photooxidation, consistent with the FTIR results. Collectively, these findings highlight the role of photooxidation in driving the release of small organic molecules rather than nano-sized particles from plastics, providing new insights into their impacts on marine ecosystems.

Keywords: Nurdle, Microplastic, Nanoplastic, Photodegradation, LC/MS, Dissolved organic matter.

Graphic abstract

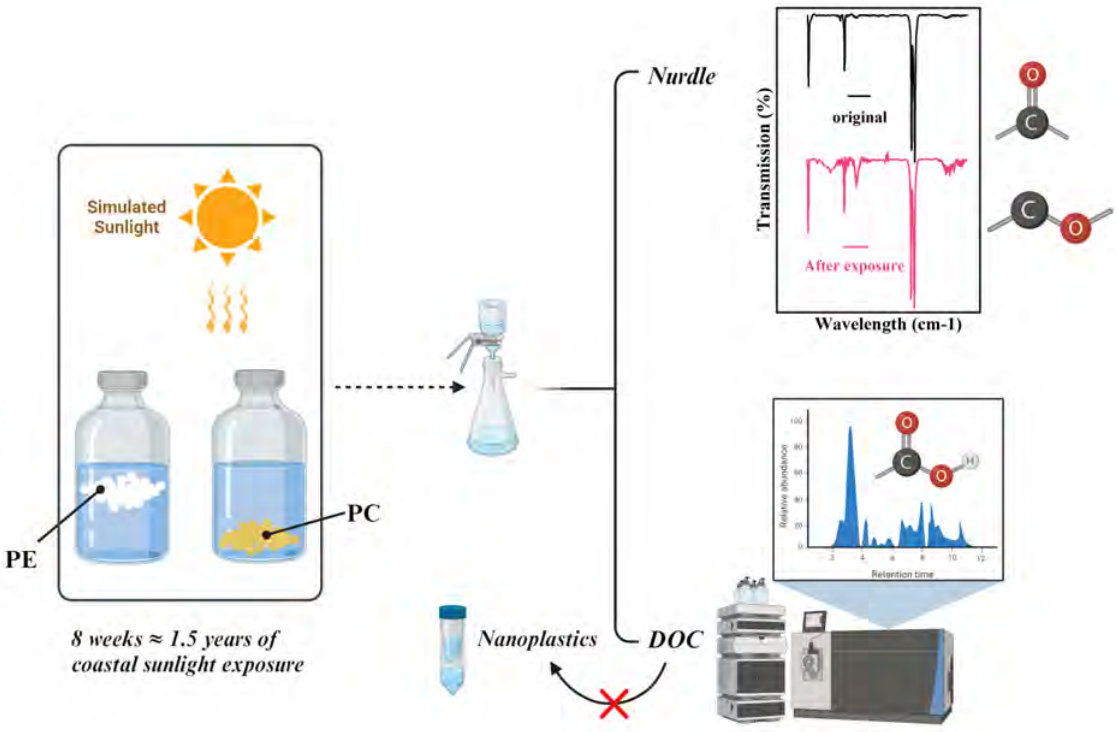

1. Introduction

In recent years, the frequent spillages of nurdles have become a growing environmental concern (Tunnell et al., 2020; de Vos et al., 2021; Sewwandi et al., 2023). As the pre-production building blocks, nurdles, also known as plastic pellets (1–5 mm diameter), are manufactured to facilitate the transportation and molding of plastic products (Hammer et al., 2012). However, nurdles often leak into the environmental throughout the plastic supply chain, particularly during transportation and distribution (Sewwandi et al., 2023). Reports of nurdle pollution date back to the early 1970s (Carpenter and Smith, 1972). Once spilled, nurdles can be readily transported by various environmental forces, such as wind and ocean currents, accumulating in marine environments (Acampora et al., 2017; Jiang et al., 2022). It is estimated that over 230,000 tons of nurdles enter the marine environment annually (de Vos et al., 2021).

These nurdles not only represent physical threat but also chemical hazard to marine life, with documented ingestion by marine fish, birds, and turtles (Ryan 1988, Gregory 2009, Clukey et al., 2017). Moreover, analyses of nurdles collected from the environment have revealed the presence of harmful contaminants, including Polycyclic Aromatic Hydrocarbons (PAHs), Polychlorinated Biphenyls (PCBs), and mercury, further underscoring the complex risks they pose to marine ecosystems (Endo et al., 2005; Antunes et al., 2013; Zhang et al., 2015; Jiang et al., 2022).

Nurdles found in marine environments exhibit a variety of polymer types, with polyethylene (PE) and polypropylene (PP) being among the most commonly reported (Zhang et al., 2015; Jiang et al., 2021). These pellets undergo weathering from environmental stressors, such as sunlight, wave action, biofouling, and temperature shifts (Turner and Holmes, 2011; Fotopoulou and Karapanagioti, 2012). Weathering introduces oxygen into the polymer chains, leading to discoloration, fragmentation, and the release of degradation byproducts into the marine

environment (Alimi et al., 2021; Andrady, 2022). For example, it has been noted that the photodegradation of common items like disposable polystyrene lids releases numerous nano-sized plastic fragments (Lambert and Wagner, 2016). Moreover, sunlight exposure of various plastics, including PE, PP, and polystyrene (PS), can lead to the release of dissolved organic matter (DOM) into the environment (Chen et al., 2019; Ward et al., 2019; L. Zhu et al., 2020; Walsh et al., 2021). For example, Walsh et al (2016) demonstrated that single-use consumer PE bags generated over 15 μM of DOM per gram of plastic per day when exposed to sunlight. with the composition influenced by plastic formulations. Despite these findings, inconsistencies remain in the kinetics and fluxes of plastic-derived DOM. Prior studies have predominantly focused on quantifying the concentration of DOM produced by small-sized microplastics (in μm scale) manufactured through various processes, while larger size plastics have been overlooked (Chen et al., 2019; Ward et al., 2019). In addition, small-sized microplastics were often made by manually trimming, to ensure size uniformity (Zhu *et al* 2020b). This trimming, while controlling size consistency, can cause physical damage to the plastics and expose fresh interior, thereby complicating direct comparisons across different polymer types. Consequently, there exists a large variability in degradation rates and the fluxes of DOM produced by different polymers. More importantly, the kinetics and molecular level information of DOM leached from plastics remain poorly understood.

High resolution mass spectrometry (HRMS) has been used to analyze plastic-derived DOMs. For example, Li et al. utilized the Liquid Chromatography Mass Spectrometer (LC/MS) method and detected hundreds of features from leachates across various plastic polymers (Li et al., 2021). However, despite these advancements, information regarding nanoplastic constituents within plastic-derived DOMs remains scarce. This scarcity arises from challenges associated with isolating nanoplastics for HRMS analysis, compounded by the inherent poor water solubility of

nano plastic particles. Thus, the characteristics and compositions of DOM leached from plastics, spanning from nano to completely dissolved substances, remain largely unexplored. Meanwhile, evidence suggests that plastic-derived DOMs can also influence microbial activity, potentially impacting marine ecosystems (L. Zhu et al., 2020). Given the increasing prevalence of plastic debris and the critical role of marine DOM in global carbon cycling as a reservoir of bioactive carbon (Hansell and Carlson, 2014), it is of great importance to deepen our understanding of how plastic degradation products affect the marine DOM dynamics.

To understand the dynamics of photooxidation and its effects on the quantity and composition of leached substances from plastics, we conducted photooxidation experiments using two types of nurdles commonly encountered in the environment: buoyant PE nurdles and non-buoyant polycarbonate (PC) nurdles, under simulated sunlight exposure. Specifically, we employed Fourier-transform infrared spectroscopy (FTIR) to detect changes in the surface chemistry of the nurdles, focusing on the formation of oxygen-containing functional groups. We also assessed the molecular formula and elemental stoichiometry of plastic-derived DOM through high-resolution mass spectrometry analysis. Our overarching objective was to elucidate the nature of photodegradation byproducts of nurdles and determine whether they exist as nanoplastics or truly dissolved compounds, providing insights into the environmental fate of plastic degradation products in marine ecosystems.

2. Materials and Methods

2.1 Polymer materials

High-density polyethylene (HDPE) and polycarbonate (PC) plastic nurdles were purchased from a commercial supplier (Pollyplastics through Amazon), and their compositions were confirmed via Fourier transform infrared spectroscopy (FTIR, Shimadzu). HDPE and PC nurdles were chosen due to their widespread global production and distinct densities, as HDPE nurdles are

buoyant on seawater, while PC nurdles are denser and sink in seawater. Prior to experimentation, the nurdles were cleaned in a 1% hydrogen peroxide solution followed by ultrasonication for 10 minutes, after which they were dried in a 60°C oven for 24 hours.

2.2 Photooxidation experiment

Artificial seawater, used for nurdle photooxidation experiment, was prepared by dissolving pre-combusted (450°C, 3h) artificial sea salt into pure water to reach a salinity of 33 ppt, ensuring the absence of residual organic matter. Photooxidation experiments were conducted by incubating nurdles under two treatments—light and dark—each in triplicate. For the light treatment, 1 g of clean nurdles (around 30 PE nurdles or 50 PC nurdles) were added to 110 mL of artificial seawater in a pre-combusted 120 mL quartz bottle, leaving 10 mL of headspace. These quartz bottles were kept in an Atlas XLS+ solar simulator, equipped with a filter-Q for artificial natural sunlight, maintaining a temperature of 33±2°C. The bottles were capped and gently shaken manually for about 10 seconds daily, and opened briefly (5 seconds) to balance pressure. The solar simulator provided an average irradiation of 5000 μmol photons/m²/s with no light/dark cycle, which is 2.5 times that of the average irradiance at noon locally at Port Aransas, TX (2000 μmol photons/m²/s). Considering the natural light-dark cycle, and the irradiation strength shift, one day in the solar simulator equates to approximately 10 days of local natural diel sunlight exposure. For the dark treatment, the same nurdles and artificial seawater were placed in pre-combusted 120 mL amber glass bottles. These bottles were kept in a closed box at 33 ± 2°C and shaken daily for 10 seconds. The experiment lasted for 8 weeks, with samples collected at each time point: day 1, week 1, week 2, week 4, week 6, and week 8. At each sampling point, nurdles were recovered by filtering the incubation solution through a pre-combusted 0.7μm glass fiber filter, and rinsed with pure water, air-dried in the hood. 20 mL of the filtrate were used to measure the bulk DOC concentration using

a total organic carbon analyzer (Shimadzu TOC-V), and the rest filtrate was collected for further analysis.

To monitor oxygen content during the experiment, 1 g of clean nurdles were incubated in 120 mL of artificial seawater in pre-combusted quartz bottles, this time with no headspace to prevent gas exchange. Bottles were placed in the Atlas XLS+ solar simulator at 33 ± 2°C under simulated natural sunlight. For the dark treatment, the same setup was used, but the quartz bottles were wrapped in aluminum foil to block light. Oxygen concentrations in the artificial seawater were measured at weeks 1 and 2 to assess changes during the early stages of photooxidation.

2.3 Characterization of nurdles

Weight of nurdles was captured through balance and color of nurdles was recorded via phone camera at each sampling timepoint. To assess the photooxidation extent to nurdles, an FTIR (IRTracer-100, Shimadzu) equipped with an attenuated total reflectance (ATR) accessory was used. The spectra of nurdles were recorded in the range of 4000 to 700 cm^{-1} at a resolution of 8 cm^{-1}, averaging 32 scans. Oxidation status of nurdles was quantified using the FTIR spectra according to published method (Brandon et al., 2016; Jiang et al., 2022). Briefly, the oxidation index for each polymer was determined by summing four individual bonds: R-OH (alcohol), C-O (ether), C=O (ketone), and C=C (vinyl). The indices were calculated by comparing the maximum absorbance value of the corresponding peak to the value of a reference peak specific to each polymer.

2.4 Identification of nanoplastics

To test the existence of nanoplastics in the solution, 50 mL of filtrated water sample of photooxidation experiment was filtrated using centrifugal filter (Centricon® Plus, 3 kDa). The cut-off of 3 kDa translates to a globular diameter of about 1-3 nm. The DOC concentrations of the concentrates and the filtrates were measured by a TOC analyzer (Shimadzu TOC-V). Due to the

concentration variation of the photooxidation filtrates and the detection limit of the TOC analyzer, ultrafiltration was only performed with groups with high DOC concentrations, i.e. PE nurdles of 4, 6, 8 weeks, and PC nurdles of 8 weeks of photooxidation.

Scanning electron microscopy (SEM, JEOL 6490) was applied to measure the surface morphology as well as the possible fragmentation of nurdles. Two nurdles were randomly selected from the samples of each time point, and then placed on double-sided carbon tape and coated with 2 nm of carbon powder to enhance conductivity. The SEM was operated at 17 kV under high vacuum, with magnifications ranging from 25× to 300×, recording a detailed examination of the surface appearance. For each individual sample, four images were captured, and the image with the best resolution for each magnification was selected and reported.

2.5 Characterization of DOC

Solid phase extraction was performed to separate DOC from the filtrates, according to the published protocols (Lu et al., 2018; Lu and Liu, 2019). Briefly, 50 mL of filtered water samples were first acidified with HCl to a pH of 2, and DOC was subsequently extracted using PPL cartridges (Agilent Bond Elut Priority Pollutant PPL cartridge, 500 mg). DOC extracts were eluted with four cartridge volumes of LC/MS grade methanol, dried and re-constituted to a final volume of 1 mL with pure water and stored at 4 °C for further analysis.

The extracted DOC was analyzed using an Ion Mobility Quadrupole Time of Flight LC/MS (IM Q-TOF LC/MS, Agilent 6560) equipped with an orthogonal electrospray ionization (ESI) source, operating in both ESI+ and ESI- modes. Briefly, in ESI+ mode, the mobile phase consisted of water with 0.1% (v/v) formic acid as phase A, and acetonitrile as phase B. DOC solutions (5-50 μL) were eluted through a StableBond C18 column (Poroshell 120 SB-C18; 2.7 μm, 2.1 × 100 mm; Agilent P/N 685775–902) at a flow rate of 0.5 mL/min. The gradient elution profile involved a

gradual increase of mobile phase B from 3% to 90% over the first 15 minutes, followed by a constant hold at 90% from 15 to 20 minutes, and a return to 3% at 21 minutes. A post-run period of 4 minutes ensured column equilibration before the subsequent injection. For ESI- mode, the mobile phase comprised water with 10 mmol/L ammonium acetate as phase A, and acetonitrile as phase B. DOC solutions (5-50 μL) were passed through a HILIC column (2.7 μm, 15 cm × 4.6 mm SUPELCO) at a flow rate of 0.5 mL/min. The elution profile involved maintaining mobile phase B at 98% for the initial minute, followed by a decrease to 95% over the subsequent 9 minutes. A post-run period of 15 minutes was allocated for column equilibration before the next injection. Approximately 0.1–0.2 μg C of DOC samples were injected per analysis, and each sample was analyzed in duplicate to ensure reliability and reproducibility of results.

The mass spectrum data were collected using MassHunter LC/MS Data Acquisition software (Version B.07.00 and B.09.00) in both ESI- and ESI+ modes. In ESI+ mode, the orthogonal electrospray ionization source (Dual Agilent Jet Stream ESI) was employed with a N_2 sheath gas temperature of 350°C at a flow rate of 12 L/min. N_2 drying gas, introduced at the source entrance, was maintained at a temperature of 225°C with a flow rate of 13 L/min and a nebulizer pressure of 45 psig. The source operated in positive mode was set to a VCap voltage of 3500 V, and a nozzle voltage of 0 V. The Q-TOF was set to positive ion polarity in MS mode, covering an MS mass range of 70–1200 m/z at an acquisition rate of 1 spectrum/s. Mass calibration was performed using reference masses of 121.050873 and 922.009798 (Agilent Tuning Mix). In ESI- mode, the ion source and sheath gas parameters remained consistent with those of ESI+ mode. However, the drying gas temperature was maintained at 225°C with a reduced flow rate of 5 L/min and a nebulizer pressure of 20 psig. The source operated in negative mode with a VCap voltage of 3500 V and a raised nozzle voltage of 2000 V. Q-TOF settings for ESI- MS were akin to those of ESI+

mode, except for the negative ion polarity and reference masses of 112.985587 and 1033.988109 (Agilent Tuning Mix).

Data analysis was performed using MassHunter Qualitative Analysis software (Version B.07.00, Service Pack 2) and relied on established methods (Lu et al., 2023, 2021, 2018; Lu and Liu, 2019). The software's "Find by Molecular Feature" function facilitated the identification of potential compounds detected in the samples. To enhance accuracy, MS spectra were converted into centroid format, with noise thresholds set at 500 and 2000 for ESI+ and ESI- modes, respectively, while signal thresholds were set at 4000 and 9000 for ESI+ and ESI- modes, respectively. A mass inaccuracy tolerance of ≤ 1.5 ppm was applied for formula assignment. Given the absence of nitrogen and phosphorus in the artificial sea salt, pure water, and plastic formulations, compound formulas were exclusively analyzed based on carbon, hydrogen, and oxygen composition. The software's "Generate Formulas" function was employed, considering exact mass and ^{13}C isotope abundance and spacing. Subsequently, the generated formulas underwent screening using custom R scripts, adhering to fundamental criteria: (1) Double Bond Equivalent (DBE) = 1 + 1/2(2C – H) ≤ 0; (2) O:C ≤ 1; (3) 0.333 ≤ H/C ≤ 2.25; and (4) isotopic spacing and abundance. Furthermore, for each molecular formula, the aromaticity index (AI) was calculated using the equation as

$$AI = (1+C-0.5O-0.5H) \div (C-0.5O)$$

with values falling between 0.5 and 0.67 designated as aromatic, and values exceeding 0.67 categorized as condensed aromatic structures.

Carbon-normalized DBE (DBE/C) were also calculated as

$$DBE/C = (1+C-0.5H) \div C$$

3. Results

3.1 Photooxidation of nurdles

The weight of both PE and PC nurdles did not change significantly after exposure to light or dark conditions ($p=0.28$ for PE, $p=0.32$ for PC, ANOVA). In addition, the appearance of nurdles remained largely unchanged after the incubation except for PC nurdles under sunlight exposure. Notably, PC nurdles turned yellower with the light exposure time increased (Figure S1), indicating photochemical reactions. Consistently, previous studies have documented instances where plastic materials exhibited darkening or yellowing after exposure to sunlight/ ultraviolet (UV) radiation (Turner and Holmes, 2011; Jiang et al., 2021). This phenomenon is commonly attributed to photooxidation, whereby oxygen is integrated into the polymer backbone chain, resulting in the formation of chromophores, thereby enhancing the polymer's coloration (Martí et al., 2020; Turner et al., 2020).

The dissolved oxygen content decreased over time in the light treatment but remained stable in the dark treatment (Figure S2). The oxygen consumption in the dark treatment was minimal, with less than 1% depletion for both polymers over 2 weeks. However, under light exposure, oxygen concentrations for PE nurdles dropped from 143.14 μM at the start of the experiment to 22.83 ± 10.37 μM at week 1 and 2.30 ± 0.63 μM at week 2. Similarly, oxygen levels for PC nurdles decreased from 143.14 μM to 63.52 ± 3.74 μM at week 1 and 22.50 ± 6.19 μM at week 2. Over the 2-week period, 98% of the dissolved oxygen was consumed for PE nurdles, and 84% for PC nurdles, indicating active oxygen involvement in photochemical reactions.

FTIR spectra of nurdles at different exposure timepoints were obtained to reflect the photochemical reactions (Figure S3). Notably, the spectra of nurdles incubated in dark conditions remained largely unaltered (Figure S3, B). In contrast, under light exposure, new peaks were generated on the spectra of both PE and PC nurdles, indicating the new functional groups induced

by the sunlight exposure. Specifically observed were peaks corresponding to hydroxyls (3300-3400 cm^{-1}), carbonyls (1690-1730 cm^{-1}), vinyl (alkenes, 1620-1650 cm^{-1}), and ethers (1100-1200 cm^{-1}).

An oxidation index of nurdles after sunlight exposure was calculated based on their FTIR spectra (Figure 1). Generally, the oxidation index for both PE and PC nurdles increased steadily with exposure time, reaching maximum values at 6 and 8 weeks, consistent with the depletion of dissolved oxygen. For example, the oxidation indices of PE nurdles increased from 0.02 ± 0.01 to 0.03 ± 0.01, 0.04 ± 0.03, 0.09 ± 0.03, 0.15 ± 0.05 (p= 0.01, T-test), and 0.21 ± 0.08 (p= 0.01, T-test), spanning from 1d to 1 week, 2 weeks, 4 weeks, 6 weeks, and 8 weeks of sunlight exposure, respectively. Similarly, the oxidation index of PC nurdles also increased from 1.58 ± 0.04 to 1.58 ± 0.03, 1.61 ± 0.05, 1.60 ± 0.06, 2.02 ± 0.12 (p= 0.03, T-test), and 2.11 ± 0.16 (p= 0.02, T-test), over the same exposure durations. The inherently higher oxidation indices of PC nurdles compared to PE nurdles can be attributed to the oxygen-containing monomers in their polymer structure, establishing a higher baseline for oxidation.

Moreover, for individual indices, in the case of PE nurdles, the oxidation index was dominated by the C=O bond throughout the exposure period, with a subsequent increase in the C-O bond observed after 4 weeks of exposure, indicating the presence of carbonyl and ether/ester groups, respectively. Conversely, for PC nurdles, the oxidation index was dominated by the C-O bond due to its inherent backbone structure, with a notable increase of the C=O bond at later stages, also after 4 weeks. The significant increase of oxidation indices for both PE and PC nurdles at 6 and 8 weeks of sunlight exposure suggests intensified oxidation reactions (Brandon et al., 2016), albeit with distinct oxidation degrees for different polymers. Notably, the prevalence of the C=O bond in the oxidation index implied the predominance of Norrish-type reactions (Alimi et al., 2021), leading to the formation of carbonyl groups on the nurdle surface.

3.2 Production of DOC

The production of DOC was observed in both sunlight and dark incubations (Figure 2, Table 1). Under dark incubation, the concentrations of DOC remained low and relatively constant, with the highest concentration occurring at 8 weeks of incubation, but barely detectable at 1 day of incubation. For example, the DOC concentrations of PE nurdles ranged from 0.17 ± 0.04 to 0.03 ± 0.02, 0.20 ± 0.06, 0.03 ± 0.00, 0.17 ± 0.09, and 0.48 ± 0.01 mg/L from 1d to 1 week, 2 weeks, 4 weeks, 6 weeks, and 8 weeks of dark incubation, respectively. Similarly, the DOC concentrations of PC nurdles ranged from 0.20 ± 0.08 to 0.11 ± 0.01, 0.07 ± 0.01, 0.06 ± 0.03, 0.15 ± 0.02, and 0.53 ± 0.02 mg/L over the same incubation durations. The detection of DOCs/leachates from plastics upon contact with incubation solutions was also reported from relevant studies (Romera-Castillo et al., 2018), representing the hydrophilic impurities and/or additives during the manufacture processes. The increase in DOC at 8 weeks of incubation under dark conditions for both plastics suggests the potential dissolution of plastics or leaching of degradation products and additives into seawater (Gewert, 2018; Guo et al., 2019), albeit at a much slower rate in the absence of sunlight exposure. Biodegradation may also contribute to this rise in DOC, considering that the dark incubation systems were not strictly sterile. However, thorough cleaning of nurdles and incubation glassware as well as the use of artificial seawater without inoculum minimizes the likelihood of microbial activity influencing these results.

In comparison to the dark controls, nurdles under sunlight exposure released much higher levels of DOC over the exposure period for both PE and PC nurdles. For example, the DOC concentrations of PE nurdles increased from 0.90 ± 0.02 to 9.73 ± 0.74, 7.21 ± 1.50, 24.59 ± 5.47, 39.27 ± 0.97, and 87.07 ± 5.67 mg/L from 1d to 1 week, 2 weeks, 4 weeks, 6 weeks, and 8 weeks of sunlight exposure, respectively. Similarly, the DOC concentrations of PC nurdles increased from 0.27 ± 0.00 to 0.15 ± 0.05, 0.44 ± 0.05, 1.13 ± 0.27, 2.91 ± 0.71, and 5.00 ± 0.67 mg/L over the

same exposure duration. The DOC concentration curves for both PE and PC nurdles show exponential patterns (Figure 2), indicating accelerating production of DOC without reaching plateau.

Notably, PE nurdles not only consumed oxygen more but also rapidly produced more DOC than PC nurdles during light exposure, reaching approximately 90 mg/L after 8 weeks of incubation—equivalent to 1% of the original PE nurdles. In contrast, PC nurdles produced much less DOC, with only 5 mg/L after the same incubation period. This disparity suggests potential differences in the environmental behaviors of PE and PC under sunlight exposure. The faster oxygen depletion and higher DOC release from PE indicate that PE may undergo more rapid photooxidation, further accelerating the breakdown of its polymer chains.

Furthermore, sunlight exposure generated more DOC than the dark incubation for both nurdles, which are consistent with previous studies showing that sunlight and UV exposure promote the degradation of plastics, increasing DOC production through the breakdown of polymer chains (Tian et al., 2019; Ward et al., 2019; K. Zhu et al., 2020). That higher DOC production and oxygen consumption under light exposure underscores the importance of photochemical processes in accelerating the weathering of plastics and releasing plastic-derived compounds into marine environments.

3.3 Identification of possible nanoplastics

The mass balance of DOC before and after centrifugal separation was provided in Table S1 Across all samples, including the incubation solution of PE nurdles after 4, 6, and 8 weeks of sunlight exposure, and PC nurdles after 8 weeks of sunlight exposure, the DOC concentrations in the filtrate, which passed through the ultrafiltration membrane (defined as ultrafiltered DOC),

accounted for approximately 100% of the bulk DOC. This result suggests that the compounds in PE and PC leachates after sunlight exposure are truly dissolved (<3000 Da).

Surface morphology analysis revealed no significant changes to the nurdles in the dark treatment (Figure 2). However, wrinkles and small cracks were observed on the PE nurdles after 6 and 8 weeks of sunlight exposure, respectively. Similarly, cracks were observed on PC nurdles after 8 weeks of sunlight exposure. These alterations indicate the occurrence of photooxidation reactions and further mechanical changes to the plastic surfaces. This observation aligns with the notable increase in oxidation indices observed at 6 and 8 weeks of sunlight exposure for both PE and PC nurdles (Figure 1). However, there were no fragments within the cracks on PE or PC nurdles, nor were particles in nanometer size. This finding is consistent with the ultrafiltration results, where hardly any nanoplastics were detected from our photooxidation experiment.

3.4 Molecular formulas of nurdle-derived DOC

The recovery of DOC through SPE showed great variability, ranging from 30% to 90%. Notably, the recovery rates of PE-DOC after 2 weeks of incubation ranged from 30% to 40%, whereas after 4 weeks, they increased notably to between 70% and 90%. However, at 6 and 8 weeks of incubation, the recovery rates fluctuated between 50% and 70%. This variability may be related to difference in concentrations and changes in the composition of plastic-derived DOC over time, with different compounds exhibiting varying affinities for the SPE cartridges at different time points. Numerous compounds were identified from the DOC of nurdles after incubation, including both dark and light treatments (Figure 3, Figure S4, Table 1, Table S1).

Due to the low concentrations of DOC in the dark treatment, compounds were only detected in the samples collected at 1 day and 8 weeks of incubation. Most of the compounds from the dark treatment for both PE and PC nurdles were identified in ESI+ mode, exhibiting similar

H/C and O/C ratios for the assigned formulas of each polymer. This result suggests a gradual leaching of impurities or plastic additives from manufacturing processes. However, some compounds leached from PE nurdles after 8 weeks of dark incubation were detected in ESI- mode, exhibiting higher O/C ratios, indicating the potential leaching of oxidation products of PE.

Under sunlight exposure, several thousand compounds were detected from nurdle-derived DOCs. More formulas were assigned in negative mode than in positive mode. The molecular masses of nurdle-derived DOCs were relatively small compared to polymer size, ranging from 102 to 716 Da for negative mode and from 102 to 926 Da for positive mode. Notably, PE nurdles yielded more formulas than PC nurdles, likely attributable to differences in DOC production. Higher DOC concentrations, or more diverse DOC molecules, may enhance compound detection, as evidenced by the absence of detected compounds in PC-derived DOC during the early exposure period. Furthermore, while more compounds were detected in positive mode for both polymers at early exposure times (e.g., 1 day, 1 week, and 2 weeks of sunlight exposure, Table 1), a shift towards more compounds detected in negative mode occurred at 4 weeks, 6 weeks, and 8 weeks of sunlight exposure. This shift suggests a significant change in the property of nurdle-derived DOCs in the middle of sunlight exposure period, indicating a potential increase in acidic compounds such as those with carboxylic groups in the later exposure stages, which are more readily ionized under negative ionization mode.

During the sunlight exposure, although the stoichiometry of nurdle-derived DOCs was closely related to the original plastic polymers' formulas, the composition and quantity of nurdle-derived DOCs differed greatly between PE and PC nurdles, while they shared similar trends from their H/C and O/C ratios. For PE-derived DOCs, at positive mode, the average O/C ratio and DBE/C significant increased at 6 and 8 weeks of exposure (from 0.22 at day 1 to 0.27 and 0.28 at

6 and 8 weeks, respectively, for O/C ratio, $p < 0.01$, ANOVA ; from 0.3 to 0.45 and 0.44 for DBE/C, $p < 0.01$, ANOVA, respectively), accompanied by a decrease in the associated H/C ratio from 1.59 to 1.23 and 1.28 during the same period. In negative mode, this trend was more pronounced, with the average O/C ratio, AI, and DBE/C increasing over time (from 0.36 to 0.36, 0.40, 0.37, 0.41, and 0.42 from 1d to 1w, 2w, 4w, 6w, and 8w of exposure for O/C ratio, $p < 0.01$, ANOVA; from 0 to 0.04, 0.09, 0.15, 0.19, and 0.20 for AI, $p < 0.01$, ANOVA; and from 0.14 to 0.20, 0.26, 0.30, 0.35, and 0.36 for DBE/C, $p < 0.01$, ANOVA, respectively), while the H/C ratio decreased (from 1.86 to 1.78, 1.67, 1.55, 1.46 and 1.46 from 1d to 1w, 2w, 4w, 6w, and 8w of exposure, $p < 0.01$, ANOVA, respectively). Conversely, for PC-derived DOCs, the high oxygen content in PC's backbone chain (various monomer formulas but all contains oxygen, e.g. $C_{14}H_{16}O_3$ and $C_{15}H_{16}O_2$) made it challenging to compare trends in the O/C ratio. Nevertheless, in positive mode, the H/C ratio of PC-derived DOCs significantly decreased from 1.52 to 1.29 at 1 day and 1.23 at 6 and 8 weeks of exposure, $p < 0.01$, ANOVA, and consistently, the associated AI and DBE/C significantly increased during the same period (from 0.24 at 1 day to 0.36 and 0.35 at 6 and 8 weeks, respectively, for AI, $p < 0.01$, ANOVA; from 0.33 at 1 day to 0.43 and 0.45 at 6 and 8 weeks, respectively, for DBE/C, $p < 0.01$, ANOVA).

4 Discussions

4.1 Photooxidation of PE and PC nurdles

Photooxidation of plastics typically initiates with the absorption of photons by the polymer, leading to the formation of free radicals (Rånby, 1989;Ainali et al., 2021; Andrady, 2022). These radicals then engage in reactions with oxygen, triggering a cascade of oxidative chain reactions (Alimi et al., 2021). While different polymers share similar principles, they may form radicals in distinct ways. For example, aromatic polymers such as PS and PC can directly absorb photons by their aromatic structures (Gewert et al., 2015). Conversely, aliphatic polyolefins like PP and PE

lack functional moieties for photon absorption, thus impurities from the manufacturing process are commonly believed to serve as the source of the initial radicals (Alimi et al., 2021).

Similar oxidative chain reactions have been observed in the photooxidation process of different polymers, resulting in the generation of comparable functional groups, such as carbonyl groups. Consistently, our FTIR results showed the oxidation of both PE and PC nurdles after sunlight exposure (Figure 1). The generation of C-O and C=O peaks in the spectra were the typical reactive intermediates of Norrish-type reactions, through the cleavage of carbon-carbon bonds upon exposure to light, leading to the incorporation of carbonyl groups into their chains. However, PE nurdles were more oxidized than PC, evidenced by the increase in C-O moieties during later stages of exposure (e.g., 6 week and 8 weeks of sunlight exposure). Moreover, the amount of DOC production and oxygen consumption from these two polymers is consistent with oxidation degree of the nurdle surface. PE nurdles generated more DOCs than PC nurdles, by an 18-fold difference, and consumed more oxygen after the same duration of sunlight exposure.

It is often thought that aromatic plastics are more susceptible to photooxidation than pure aliphatic plastics, owing to their content of conjugated double bonds and aromatic rings (Gewert et al., 2015), facilitating the generation of reactive intermediates, and promoting resonance stabilization. However, our results did not support this assumption, as PE exhibited greater oxidation than PC. Given that both PE and PC nurdles were subjected to identical light intensity and temperature conditions, and considering that they were unaltered pre-products devoid of common additives, we propose an alternative explanation for the observed discrepancy. The difference in buoyancy between the two polymers may have played a key role. The density of PE is much lighter than PC as compared to water, leading to PE floating on water surface while PC in the bottom of the water. This spatial separation may have influenced oxygen accessibility, with PE

nurdles at the air-water interface having greater access to atmospheric oxygen compared to PC nurdles at the bottom. This is consistent with our observation that 98% of the dissolved oxygen was depleted within 2 weeks for PE nurdles, compared to 84% for PC nurdles (Figure S2). The dissolved oxygen might be depleted in our incubation system after 2 weeks. Despite briefly opening the lids each day to balance pressure, oxygen replenishment may have been insufficient for the submerged PC nurdles. In contrast, PE nurdles floating at the surface likely had more consistent access to oxygen from the headspace, promoting more extensive photooxidation. Additionally, the rate of photooxidation is affected by the oxygen concentration (Andrady, 2022), and the buoyancy difference may have resulted in varying exposure to both UV radiation and dissolved oxygen, with PE nurdles receiving higher doses of each. As a result, even though PC is an aromatic polymer, its photooxidation was less pronounced than that of aliphatic PE. Alternatively, PE may simply be more photosensitive than PC, resulting in higher DOC production. Although PC is an aromatic polymer, its known UV-blocking properties, commonly exploited in sunglasses and engineered materials, may have contributed to its lower photooxidation. Further studies are needed to investigate the role of dissolved oxygen in the photooxidation of different plastic polymers.

While aromatic polymers are generally considered more prone to photooxidation, much of the evidence for this assumption comes from studies on PS rather than other aromatic plastics like PC. PS microplastics are frequently reported to be highly susceptible to weathering and to produce more leachates or DOC than polyolefins under similar conditions (Song et al., 2017, 2020; Ward et al., 2019; L. Zhu et al., 2020). For example, Song et al found that expanded PS (EPS) experienced fragmentation easily when exposed to sunlight (Song et al., 2020, 2017), and Zhu et al., found that EPS produced more DOCs than PE and PP under same simulated sunlight exposure. However, EPS has a distinct structure compared to regular PS, containing air-filled bubbles that make it

lightweight and more prone to fragmentation. In our study, we selected polymers with similar size, shape, and manufacturing processes to reduce potential structural differences and ensure more comparable results. Our results show that aliphatic plastics, such as PE, were more susceptible to photooxidation than aromatic PC under the same experimental conditions. This discrepancy highlights the complexity of plastic weathering dynamics. Further investigations comparing expanded versus non-expanded polymers or examining degradation in air versus water environments will be crucial to better understand the differing photodegradation behaviors of aliphatic and aromatic plastics.

4.2 Major forms of photooxidation products

Sunlight exposure triggers oxidation reactions on plastics, potentially altering their mechanical integrity (Barnes et al., 2009; Song et al., 2020; Menzel et al., 2022). Previous studies have shown the production of nanoscale particles through fragmentation during the photodegradation of plastics such as PE, PP, and PS. For instance, Menzel et al. confirmed the generation of nanoplastics from low-density PE following accelerated sunlight exposure using complementary analytical methods (Menzel et al., 2022). Similarly, Song et al. detected thousands of nanoplastic particles produced by PE, PP, and EPS plastics after UV exposure followed by mechanical abrasion with sand (Song et al., 2020). While it was previously believed that photooxidation led to cross-linking and chain scission reactions on the plastic surface, gradually weakening and embrittling the material and potentially causing macro- and micro-fragmentation (Gewert et al., 2015; Karlsson et al., 2018). However, after 8 weeks of accelerated sunlight exposure, we found that the predominant photooxidation products from nurdles were dissolved compounds, with no evidence of nanoplastics. This outcome may be attributed to the use of intact large nurdles and the absence of mechanical forces during the photooxidation process.

In related studies focusing on microplastic photodegradation, plastic materials were often trimmed or ground, potentially deteriorating their physical properties and favoring fragmentation (K. Zhu et al., 2020; L. Zhu et al., 2020; Menzel et al., 2022). Moreover, to mimic natural conditions, mechanical forces such as abrasion with sand or stirring with bars were frequently applied during light exposure (Song et al., 2020, 2017). In contrast, our study utilized limited agitation and intact nurdles, which have larger dimensions (5 mm in diameter) compared to typical microplastics used in similar studies. In our study, the oxidation of nurdles may increase the hydrophilicity of the surface, facilitating the dissolution of small, oxidized molecules into ambient solutions. However, this process relies solely on passive diffusion based on solubility, with small soluble compounds ending up in the solution phase. In contrast, nanoplastics, due to their larger size compared to the compounds, remained attached to the nurdles in the absence of necessary mechanical forces.

Limited fragmentation during photooxidation process was also reported. Our findings align with those of previous studies (Andrady, 2022; Tuttle et al., 2024). For example, Svedin reported no fragmentation of low-density polyethylene (LDPE) and polypropylene (PP) under simulated sunlight exposure (Svedin, 2020), while Kalogerakis et al. similarly found no fragmentation of PE and PP plastics after 6 months of natural solar weathering (Kalogerakis et al., 2017), both experiments conducted without strong mechanical forces such as abrasions or continuous stirring. Overall, our results show that without mechanical forces involved essentially no nanoplastics can be produced from primary plastics under pure photooxidation. Further work applying different degrees of mechanical forces and on plastics on different weathering stages may be needed in order to gain further understanding how nanoplastics are formed in natural environments.

4.3 Molecular-level information of photooxidation products

It is challenging to compare the production of DOCs from plastics after photooxidation between different studies due to variations in applied sunlight intensity and the types of plastic materials used. However, for a preliminary assessment, the concentration of PE-derived DOCs in our study appeared to be within a similar magnitude as reported in other studies. For instance, Zhu et al. measured the DOC production from different polymers after exposure equivalent to approximately 68 days of solar irradiation at the subtropical ocean gyre surface and detected 4.76 mg of DOC per gram of PE carbon (L. Zhu et al., 2020). In our study, conducted at the solar intensity as a similar latitude as the subtropical ocean gyre (20°–30° latitude), the 68-day exposure period corresponded to the 1-week sampling point, we observed a concentration of around 10 mg of DOC per gram of PE nurdle carbon.

HRMS analysis can elucidate the molecular information of plastic-derived DOCs (Gewert et al., 2018; Walsh et al., 2021; Stubbins et al., 2023). The stoichiometry of DOCs differed between PE and PC nurdles, with PC-DOCs exhibiting higher oxygen content due to the presence of oxygen in PC chains. Over exposure time, the assigned formulas of DOCs from both nurdles showed an increase in O/C ratios but a decrease in H/C ratios, suggesting a progressive enrichment of oxygen in the DOC composition. This enrichment likely resulted from the incorporation of more oxygen into plastic chains, replacing hydrogen atoms through chain scission reactions induced by sunlight exposure. Consistently, the FTIR results revealed a gradual addition of oxygen to plastic chains with exposure time (Figure 1). Furthermore, an increase in the number of formulas assigned in negative mode at later exposure stages indicated a rise in carboxylic acid products of nurdle-derived DOCs, contributing to the elevated oxygen content. Our findings align with previous studies by Gewert et al., who identified chain scission products, primarily dicarboxylic acids, from plastic pellets following UV exposure. It has also been demonstrated that carboxylic and dicarboxylic acids

are among the most prevalent and stable products of PE photodegradation, as their structures exhibit greater resilience to sunlight exposure compared to ketones, aldehydes, and alcohols (Fachrul et al., 2021).

The stoichiometry of nurdle-derived DOCs also offers some clues on their bioavailability. Some studies suggested that molecules with low hydrogen content, indicated by a low H/C ratio, are less readily available to microorganisms (Kim et al., 2006), with those possessing an H/C ratio ≤ 1.5 considered resistant to degradation (D'Andrilli et al., 2015). Therefore, the observed decrease in H/C ratio of nurdle-derived DOCs over the duration of sunlight exposure in both ESI modes may indicate an increase in their recalcitrance over time. Moreover, the concurrent increase of AI and DBE/C of the DOC formulas suggested the accumulation of carboxyl-rich alicyclic molecules (CRAM)-like compounds (Lu et al., 2021; Stubbins et al., 2023), which might affect the environmental behavior of nurdle-derived DOCs, including their residence time and bioavailability (L. Zhu et al., 2020). Similar findings were reported by Stubbins et al. (2023), who identified CRAM-like formulas in PE, PP, and expanded polystyrene (EPS)-derived DOCs after sunlight exposure, highlighting their varying bioavailabilities for microbial degradation. The CRAM-like compounds are known to be refractory in aquatic environments (Hertkorn et al., 2006), suggesting that nurdle-derived DOCs may be less susceptible to biodegradation and more recalcitrant in nature.

5 Environmental implications

The findings of this study revealed the significant production of DOC from both PE and PC nurdles into the ambient environment after sunlight exposure, with PE yielding 18 times more DOC than PC nurdles. Importantly, the predominant form of nurdle-derived DOC was found to be truly dissolved compounds, rather than plastic particles in nanometer scales. Molecular signatures of nurdle-derived DOCs were influenced by their polymer composition, yet displayed a shared

trend characterized by an increase in CRAM-like and carboxylic acid structures with prolonged exposure time. This study underscores the role of oxygen availability, influenced by plastic density, in shaping photodegradation pathways and highlights the efficacy of high-resolution mass spectrometry in analyzing plastic photodegradation products. Further research on photodegradation and environmental weathering products of plastics using raw plastic materials and complementary analytical approaches is needed for a comprehensive understanding of the fate and impacts of plastic pollution in natural environments. Also needed is to evaluate bioavailability of plastic-derived DOC to microorganisms in marine environments.

Acknowledgments

We thank Dr Kenny Befus and Dr. Elizabeth Catlos for their help with the Low-Vacuum Scanning Electron Microscope. We thank Dr. Ryan Hladyniuk from the UTMSI Core Facility Lab for helping with LC/MS analysis. This work was supported by the Matagorda Bay Mitigation Trust (RFP# 2022-2023-1).

References

Acampora, H., Berrow, S., Newton, S., O'Connor, I., 2017. Presence of plastic litter in pellets from Great Cormorant (Phalacrocorax carbo) in Ireland. Marine Pollution Bulletin 117, 512–514. https://doi.org/10.1016/j.marpolbul.2017.02.015

Ainali, N.M., Bikiaris, D.N., Lambropoulou, D.A., 2021. Aging effects on low- and high-density polyethylene, polypropylene and polystyrene under UV irradiation: an insight into decomposition mechanism by Py-GC/MS for microplastic analysis. Journal of Analytical and Applied Pyrolysis 105207. https://doi.org/10.1016/j.jaap.2021.105207

Alimi, O.S., Claveau-Mallet, D., Kurusu, R.S., Lapointe, M., Bayen, S., Tufenkji, N., 2021. Weathering pathways and protocols for environmentally relevant microplastics and

nanoplastics: What are we missing? Journal of Hazardous Materials 126955. https://doi.org/10.1016/j.jhazmat.2021.126955

Andrady, A.L., 2022. Weathering and fragmentation of plastic debris in the ocean environment. Marine Pollution Bulletin 180, 113761. https://doi.org/10.1016/j.marpolbul.2022.113761

Antunes, J.C., Frias, J.G.L., Micaelo, A.C., Sobral, P., 2013. Resin pellets from beaches of the Portuguese coast and adsorbed persistent organic pollutants. Estuarine, Coastal and Shelf Science 130, 62–69. https://doi.org/10.1016/j.ecss.2013.06.016

Barnes, D.K.A., Galgani, F., Thompson, R.C., Barlaz, M., 2009. Accumulation and fragmentation of plastic debris in global environments. Philosophical Transactions of the Royal Society B: Biological Sciences 364, 1985–1998. https://doi.org/10.1098/rstb.2008.0205

Brandon, J., Goldstein, M., Ohman, M.D., 2016. Long-term aging and degradation of microplastic particles: Comparing in situ oceanic and experimental weathering patterns. Marine pollution bulletin 110, 299–308. https://doi.org/10.1016/j.marpolbul.2016.06.048

Carpenter, E.J., Smith, K.L., 1972. Plastics on the Sargasso Sea surface. Science 175, 1240–1241.

Chen, Q., Allgeier, A., Yin, D., Hollert, H., 2019. Leaching of endocrine disrupting chemicals from marine microplastics and mesoplastics under common life stress conditions. Environment International 130, 104938. https://doi.org/10.1016/j.envint.2019.104938

Clukey, K.E., Lepczyk, C.A., Balazs, G.H., Work, T.M., Lynch, J.M., n.d. Investigation of plastic debris ingestion by four species of sea turtles collected as bycatch in pelagic Pacific longline fisheries. Marine Pollution Bulletin. https://doi.org/10.1016/j.marpolbul.2017.04.064

D'Andrilli, J., Cooper, W.T., Foreman, C.M., Marshall, A.G., 2015. An ultrahigh-resolution mass spectrometry index to estimate natural organic matter lability. Rapid Commun Mass Spectrom 29, 2385–2401. https://doi.org/10.1002/rcm.7400

de Vos, A., Aluwihare, L., Youngs, S., DiBenedetto, M.H., Ward, C.P., Michel, A.P.M., Colson, B.C., Mazzotta, M.G., Walsh, A.N., Nelson, R.K., Reddy, C.M., James, B.D., 2021. The M/V X-Press Pearl nurdle spill: Contamination of burnt plastic and unburnt nurdles along Sri Lanka's beaches. ACS Environ. Au. https://doi.org/10.1021/acsenvironau.1c00031

Endo, S., Takizawa, R., Okuda, K., Takada, H., Chiba, K., Kanehiro, H., Ogi, H., Yamashita, R., Date, T., 2005. Concentration of polychlorinated biphenyls (PCBs) in beached resin pellets: Variability among individual particles and regional differences. Marine Pollution Bulletin 50, 1103–1114. https://doi.org/10.1016/j.marpolbul.2005.04.030

Fachrul, M.F., Rinanti, A., Salmiati, S., Sunaryo, T., 2021. Degradation of polyethylene plastic waste by indigenous microbial consortium and fungi. Indonesian Journal of Urban and Environmental Technology 5, 86–103. https://doi.org/10.25105/urbanenvirotech.v5i1.10749

Fotopoulou, K.N., Karapanagioti, H.K., 2012. Surface properties of beached plastic pellets. Marine Environmental Research 81, 70–77. https://doi.org/10.1016/j.marenvres.2012.08.010

Gewert, B., 2018. Chemical Pollutants Released to the Marine Environment by Degradation of Plastic Debris. Doctoral dissertation, Department of Environmental Science and Analytical Chemistry, Stockholm University.

Gewert, B., Plassmann, M., Sandblom, O., MacLeod, M., 2018. Identification of chain scission products released to water by plastic exposed to Ultraviolet light. Environ. Sci. Technol. Lett. https://doi.org/10.1021/acs.estlett.8b00119

Gewert, B., Plassmann, M.M., MacLeod, M., 2015. Pathways for degradation of plastic polymers floating in the marine environment. Environ. Sci.: Processes Impacts 17, 1513–1521. https://doi.org/10.1039/C5EM00207A

Gregory, M.R., 2009. Environmental implications of plastic debris in marine settings—entanglement, ingestion, smothering, hangers-on, hitch-hiking and alien invasions. Philosophical Transactions of the Royal Society B: Biological Sciences 364, 2013–2025. https://doi.org/10.1098/rstb.2008.0265

Guo, H., Zheng, X., Ru, S., Luo, X., Mai, B., 2019. The leaching of additive-derived flame retardants (FRs) from plastics in avian digestive fluids: The significant risk of highly lipophilic FRs. Journal of Environmental Sciences, SI: Recent advances in Environmental Sciences 85, 200–207. https://doi.org/10.1016/j.jes.2019.06.013

Hammer, J., Kraak, M.H.S., Parsons, J.R., 2012. Plastics in the marine environment: the dark side of a modern gift. Rev Environ Contam Toxicol 220, 1–44. https://doi.org/10.1007/978-1-4614-3414-6_1

Hansell, D.A., Carlson, C.A., 2014. Biogeochemistry of marine dissolved organic matter. Ch. 2. Academic press.

Hertkorn, N., Benner, R., Frommberger, M., Schmitt-Kopplin, P., Witt, M., Kaiser, K., Kettrup, A., Hedges, J.I., 2006. Characterization of a major refractory component of marine dissolved organic matter. Geochimica et Cosmochimica Acta 70, 2990–3010. https://doi.org/10.1016/j.gca.2006.03.021

Jiang, X., Conner, N., Lu, K., Tunnell, J.W., Liu, Z., 2022. Occurrence, distribution, and associated pollutants of plastic pellets (nurdles) in coastal areas of South Texas. Science of The Total Environment 842, 156826. https://doi.org/10.1016/j.scitotenv.2022.156826

Jiang, X., Lu, K., Tunnell, J.W., Liu, Z., 2021. The impacts of weathering on concentration and bioaccessibility of organic pollutants associated with plastic pellets (nurdles) in coastal environments. Marine Pollution Bulletin 170, 112592. https://doi.org/10.1016/j.marpolbul.2021.112592

Kalogerakis, N., Karkanorachaki, K., Kalogerakis, G.C., Triantafyllidi, E.I., Gotsis, A.D., Partsinevelos, P., Fava, F., 2017. Microplastics generation: Onset of fragmentation of polyethylene films in marine environment mesocosms. Front. Mar. Sci. 4. https://doi.org/10.3389/fmars.2017.00084

Karlsson, T.M., Hassellöv, M., Jakubowicz, I., 2018. Influence of thermooxidative degradation on the in situ fate of polyethylene in temperate coastal waters. Marine Pollution Bulletin 135, 187–194. https://doi.org/10.1016/j.marpolbul.2018.07.015

Kim, S., Kaplan, L.A., Hatcher, P.G., 2006. Biodegradable dissolved organic matter in a temperate and a tropical stream determined from ultra-high resolution mass spectrometry. Limnology and Oceanography 51, 1054–1063. https://doi.org/10.4319/lo.2006.51.2.1054

Lambert, S., Wagner, M., 2016. Formation of microscopic particles during the degradation of different polymers. Chemosphere 161, 510–517. https://doi.org/10.1016/j.chemosphere.2016.07.042

Li, Y., Lu, Z., Abrahamsson, D.P., Song, W., Yang, C., Huang, Q., Wang, J., 2021. Non-targeted analysis for organic components of microplastic leachates. Science of The Total Environment 151598. https://doi.org/10.1016/j.scitotenv.2021.151598

Lu, K., Gardner, W.S., Liu, Z., 2018. Molecular structure characterization of riverine and coastal dissolved organic matter with ion mobility quadrupole time-of-flight LCMS (IM Q-TOF LCMS). Environ. Sci. Technol. 52, 7182–7191. https://doi.org/10.1021/acs.est.8b00999

Lu, K., Li, X., Chen, H., Liu, Z., 2021. Constraints on isomers of dissolved organic matter in aquatic environments: Insights from ion mobility mass spectrometry. Geochimica et Cosmochimica Acta 308, 353–372. https://doi.org/10.1016/j.gca.2021.05.007

Lu, K., Liu, Z., 2019. Molecular level analysis reveals changes in chemical composition of dissolved organic matter from south Texas rivers after high flow events. Front. Mar. Sci. 6. https://doi.org/10.3389/fmars.2019.00673

Lu, K., Xue, J., Guo, L., Liu, Z., 2023. The bio- and thermal lability of dissolved organic matter as revealed by high-resolution mass spectrometry and thermal chemical analyses. Marine Chemistry 250, 104184. https://doi.org/10.1016/j.marchem.2022.104184

Martí, E., Martin, C., Galli, M., Echevarría, F., Duarte, C.M., Cózar, A., 2020. The colors of the ocean plastics. Environ. Sci. Technol. acs.est.9b06400. https://doi.org/10.1021/acs.est.9b06400

Menzel, T., Meides, N., Mauel, A., Mansfeld, U., Kretschmer, W., Kuhn, M., Herzig, E.M., Altstädt, V., Strohriegl, P., Senker, J., Ruckdäschel, H., 2022. Degradation of low-density polyethylene to nanoplastic particles by accelerated weathering. Science of The Total Environment 826, 154035. https://doi.org/10.1016/j.scitotenv.2022.154035

Rånby, B., 1989. Photodegradation and photo-oxidation of synthetic polymers. Journal of Analytical and Applied Pyrolysis 15, 237–247. https://doi.org/10.1016/0165-2370(89)85037-5

Romera-Castillo, C., Pinto, M., Langer, T.M., Álvarez-Salgado, X.A., Herndl, G.J., 2018. Dissolved organic carbon leaching from plastics stimulates microbial activity in the ocean. Nature Communications 9, 1430. https://doi.org/10.1038/s41467-018-03798-5

Ryan, P.G., 1988. Effects of ingested plastic on seabird feeding: Evidence from chickens. Marine Pollution Bulletin 19, 125–128. https://doi.org/10.1016/0025-326X(88)90708-4

Sewwandi, M., Keerthanan, S., Perera, K.I., Vithanage, M., 2023. Plastic nurdles in marine environments due to accidental spillage. Microplastics in the Ecosphere: Air, Water, Soil, and Food, pp. 415–432. https://doi.org/10.1002/9781119879534.ch26

Song, Y.K., HONG, S.H., Eo, S., Han, G.M., Shim, W.J., 2020. Rapid production of micro- and nanoplastics by fragmentation of expanded polystyrene exposed to sunlight. Environ. Sci. Technol. https://doi.org/10.1021/acs.est.0c02288

Song, Y.K., Hong, S.H., Jang, M., Han, G.M., Jung, S.W., Shim, W.J., 2017. Combined effects of UV exposure duration and mechanical abrasion on microplastic fragmentation by polymer type. Environ. Sci. Technol. 51, 4368–4376. https://doi.org/10.1021/acs.est.6b06155

Stubbins, A., Zhu, L., Zhao, S., Spencer, R.G.M., Podgorski, D.C., 2023. Molecular signatures of dissolved organic matter generated from the photodissolution of microplastics in sunlit seawater. Environ. Sci. Technol. 57, 20097–20106. https://doi.org/10.1021/acs.est.1c03592

Svedin, J., 2020. Photodegradation of macroplastics to microplastics : A laboratory study on common litter found in urban areas.

Tian, L., Chen, Q., Jiang, W., Wang, L., Xie, H., Kalogerakis, N., Ma, Y., Ji, R., 2019. A carbon-14 radiotracer-based study on the phototransformation of polystyrene nanoplastics in water versus in air. Environ. Sci.: Nano 6, 2907–2917. https://doi.org/10.1039/C9EN00662A

Tunnell, J.W., Dunning, K.H., Scheef, L.P., Swanson, K.M., 2020. Measuring plastic pellet (nurdle) abundance on shorelines throughout the Gulf of Mexico using citizen scientists: Establishing a platform for policy-relevant research. Marine Pollution Bulletin 151, 110794. https://doi.org/10.1016/j.marpolbul.2019.110794

Turner, A., Arnold, R., Williams, T., 2020. Weathering and persistence of plastic in the marine environment: Lessons from LEGO. Environmental Pollution 262, 114299. https://doi.org/10.1016/j.envpol.2020.114299

Turner, A., Holmes, L., 2011. Occurrence, distribution and characteristics of beached plastic production pellets on the island of Malta (central Mediterranean). Marine Pollution Bulletin 62, 377–381. https://doi.org/10.1016/j.marpolbul.2010.09.027

Tuttle, E., Wiman, C., Muñoz, S., Law, K.L., Stubbins, A., 2024. Sunlight-Driven photochemical removal of polypropylene microplastics from surface waters follows linear kinetics and does not result in fragmentation. Environ. Sci. Technol. 58, 5461–5471. https://doi.org/10.1021/acs.est.3c07161

Walsh, A.N., Reddy, C.M., Niles, S.F., McKenna, A.M., Hansel, C.M., Ward, C.P., 2021. Plastic formulation is an emerging control of its photochemical fate in the ocean. Environ. Sci. Technol. 55, 12383–12392. https://doi.org/10.1021/acs.est.1c02272

Ward, C.P., Armstrong, C.J., Walsh, A.N., Jackson, J.H., Reddy, C.M., 2019. Sunlight converts polystyrene to carbon dioxide and dissolved organic carbon. Environ. Sci. Technol. Lett. https://doi.org/10.1021/acs.estlett.9b00532

Zhang, W., Ma, X., Zhang, Z., Wang, Y., Wang, J., Wang, J., Ma, D., 2015. Persistent organic pollutants carried on plastic resin pellets from two beaches in China. Marine pollution bulletin 99, 28–34. https://doi.org/10.1016/j.marpolbul.2015.08.002

Zhu, K., Jia, H., Sun, Y., Dai, Y., Zhang, C., Guo, X., Wang, T., Zhu, L., 2020. Long-term phototransformation of microplastics under simulated sunlight irradiation in aquatic environments: Roles of reactive oxygen species. Water Research 173, 115564. https://doi.org/10.1016/j.watres.2020.115564

Zhu, L., Zhao, S., Bittar, T.B., Stubbins, A., Li, D., 2020. Photochemical dissolution of buoyant microplastics to dissolved organic carbon: Rates and microbial impacts. Journal of Hazardous Materials 383, 121065. https://doi.org/10.1016/j.jhazmat.2019.121065

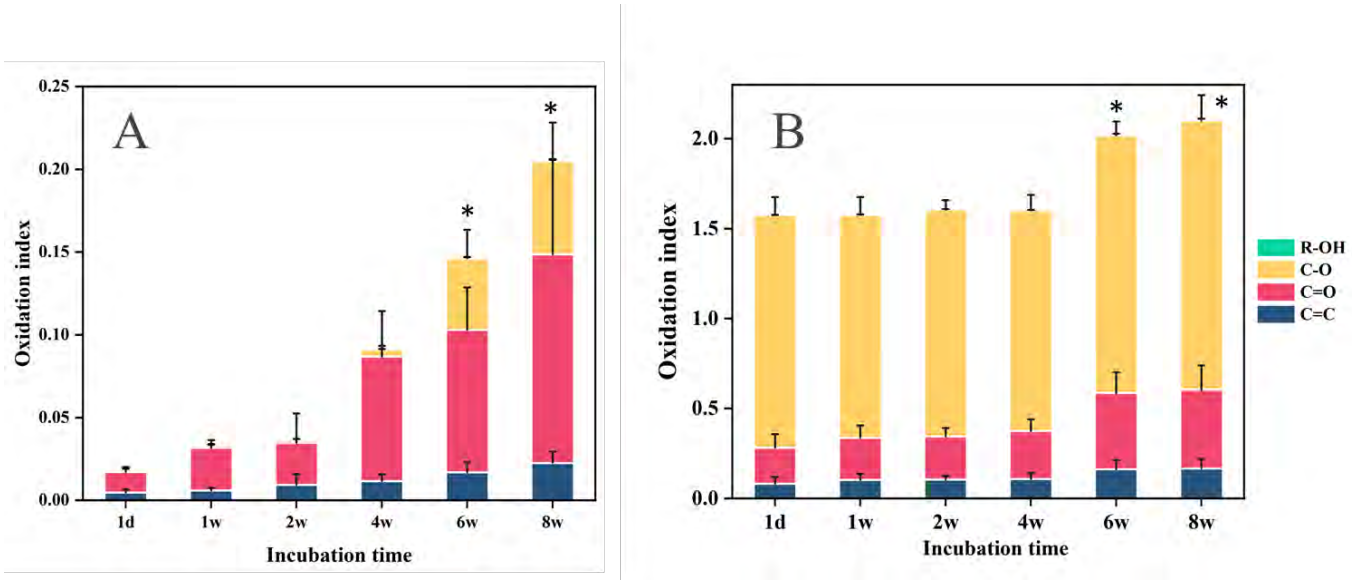

Figure 1. Oxidation indices of PE (A) and PC (B) nurdles after simulated sunlight exposure, calculated by summing four individual bonds: R-OH (alcohol), C-O (ether), C=O (ketone), and C=C (vinyl).

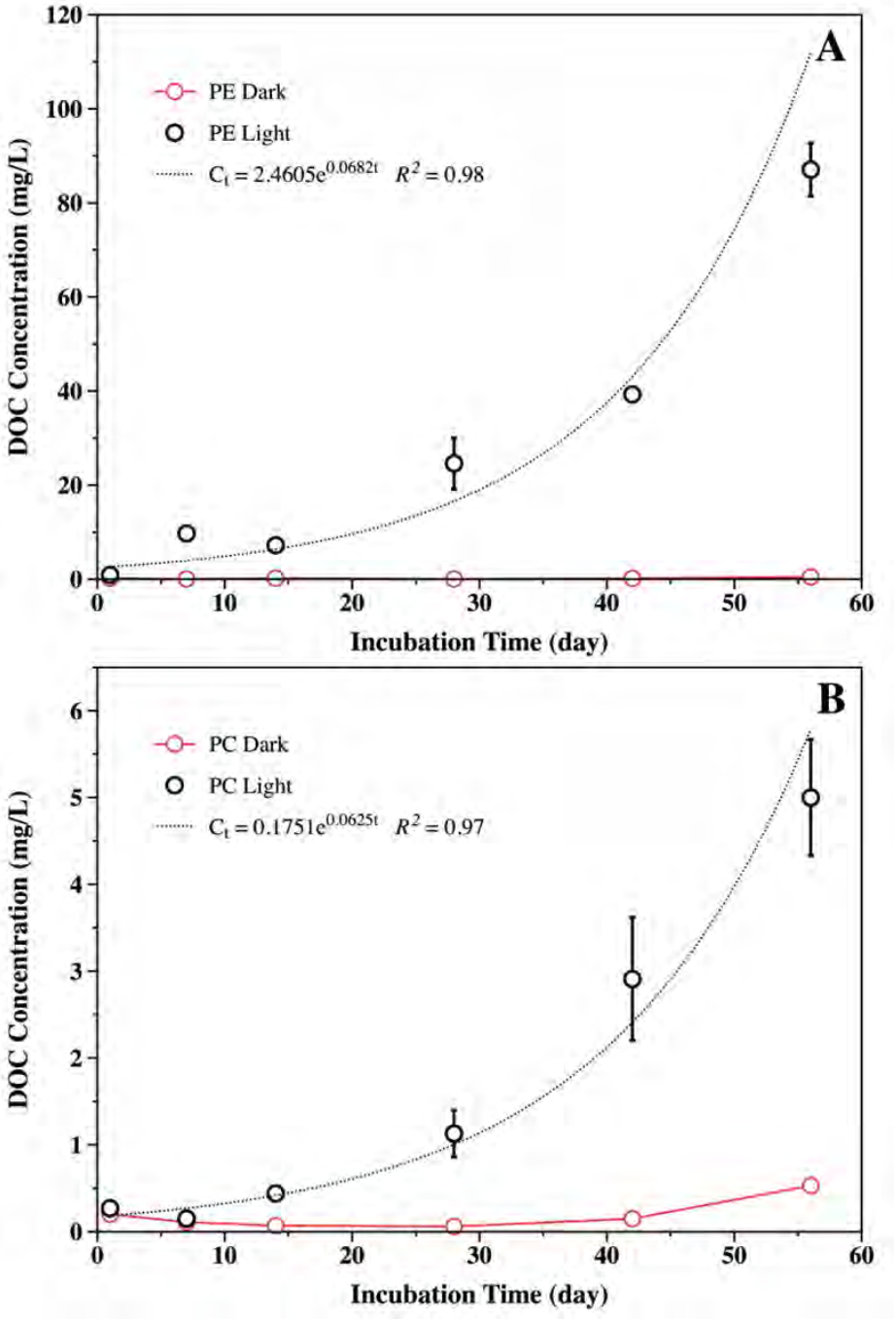

Figure 2. Total dissolved organic carbon (TDOC) production from polyethylene (PE, A), and polycarbonate (PC, B) nurdles in artificial seawater in both light and the dark.

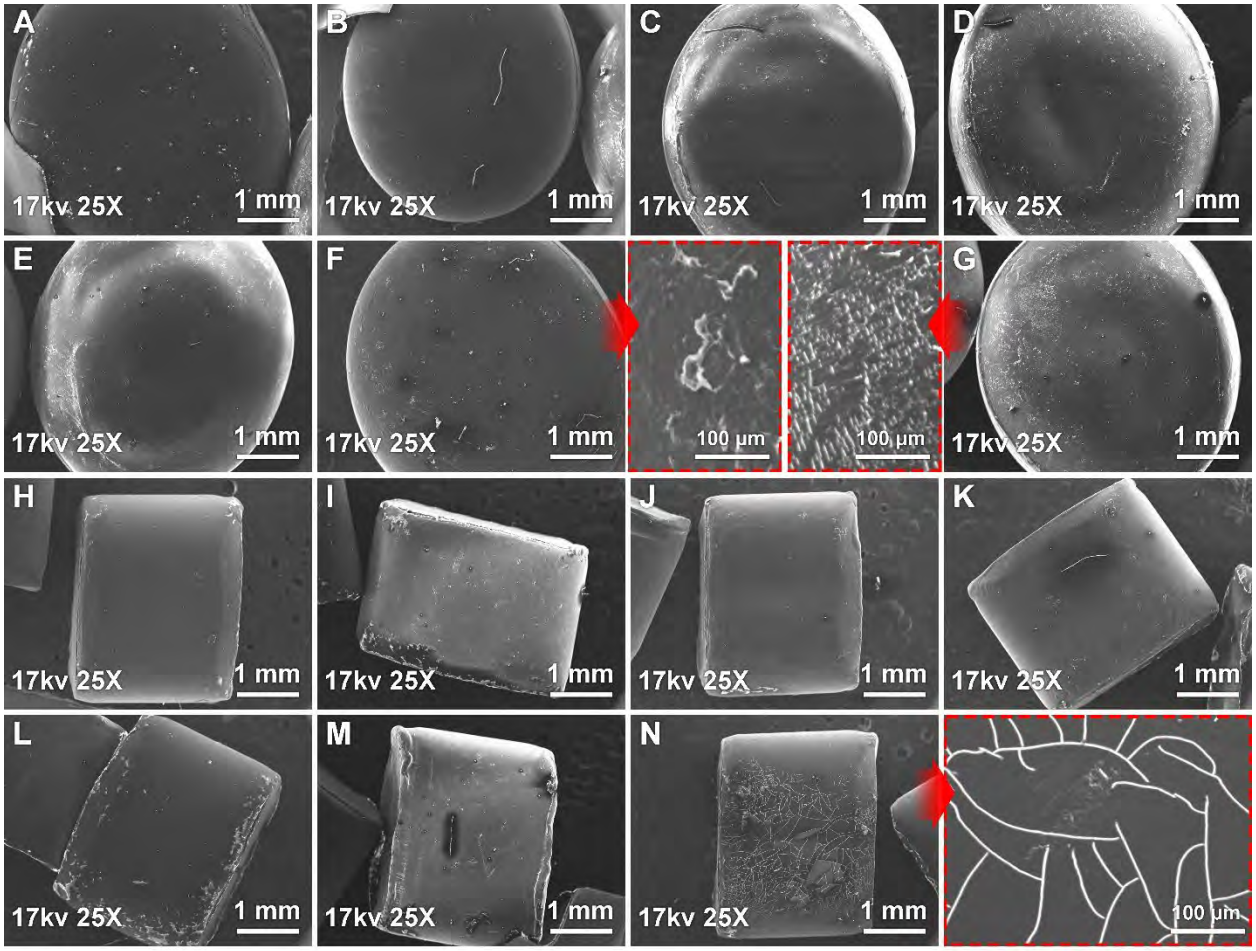

Figure 3. SEM images of surface morphology with magnification of 25x by increasing sunlight exposure time for PE (A,B, C, D, E, F, G at 1d, 1w, 2w, 4w, 6w, 8w, respectively, with 300x magnification of 6w and 8w showing with arrow) and PC (H, I, J, K, L, M, N at 1d, 1w, 2w, 4w, 6w, 8w, respectively, with 300x magnification of 8w showing with arrow) nurdles.

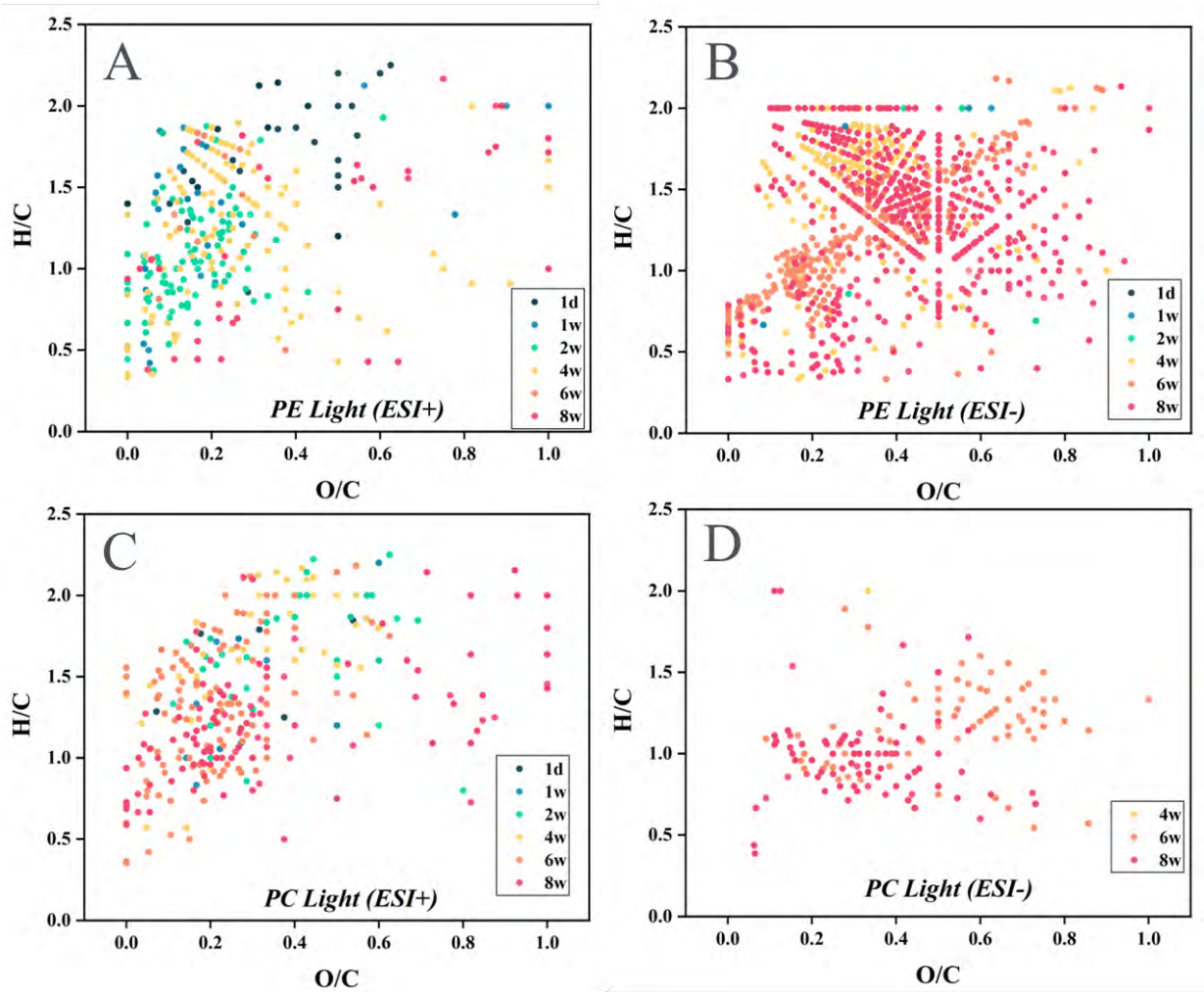

Figure 4. van Krevelen diagrams for CHO molecular formulas produced during the photooxidation of nurdles in artificial seawater: (A) PE-derived DOCs under ESI+ mode; (B) PE-derived DOCs under ESI- mode; (C) PC-derived DOCs under ESI+ mode; (D) PC-derived DOCs under ESI- mode.

Table 1. Element stoichiometry of CHO molecular formulas produced during the photooxidation of nurdles in artificial seawater.

		PE					
	Incubation time	**1d**	**1w**	**2w**	**4w**	**6w**	**8w**
ESI+	**DOC-production (mg/L)**	0.90 ± 0.02	9.73 ± 0.74	7.21 ± 1.50	24.59 ± 5.47	39.27 ± 0.97	87.07 ± 5.67
	Assigned formulas	93	328	335	372	77	97
	Average molecular mass	232.11 ± 65.86	306.61 ± 133.01	315.45 ± 127.07	232.99 ± 69.75	280.32 ± 134.53	266.43 ± 106.21
	Average H/C	1.59 ± 0.31	1.21 ± 0.41	1.08 ± 0.34	1.23 ± 0.42	1.23 ± 0.48	1.28 ± 0.50
	Average O/C	0.26 ± 0.15	0.19 ± 0.15	0.17 ± 0.11	0.27 ± 0.18	0.28 ± 0.32	0.47 ± 0.32
	Average AI	0.22 ± 0.17	0.39 ± 0.22	0.47 ± 0.19	0.39 ± 0.23	0.38 ± 0.29	0.30 ± 0.31
	Average DBE/C	0.30 ± 0.17	0.45 ± 0.20	0.51 ± 0.17	0.47 ± 0.21	0.45 ± 0.23	0.44 ± 0.23
ESI-	**Assigned formulas**	1	166	180	1596	2714	1863
	Average molecular mass	274.18	275.03 ± 149.14	291.52 ± 165.75	324.90 ± 146.88	342.00 ± 154.98	330.41 ± 156.21
	Average H/C	1.86	1.78 ± 0.18	1.67 ± 0.25	1.55 ± 0.32	1.46 ± 0.33	1.46 ± 0.41
	Average O/C	0.36	0.36 ± 0.12	0.40 ± 0.11	0.37 ± 0.13	0.41 ± 0.17	0.42 ± 0.18
	Average AI	0	0.04 ± 0.09	0.09 ± 0.14	0.15 ± 0.18	0.19 ± 0.19	0.20 ± 0.22
	Average DBE/C	0.14	0.20 ± 0.09	0.26 ± 0.14	0.30 ± 0.16	0.35 ± 0.16	0.36 ± 0.20

Table 1. (cont.) Element stoichiometry of CHO molecular formulas produced during the photooxidation of nurdles in artificial seawater.

		PC					
	Incubation time	**1d**	**1w**	**2w**	**4w**	**6w**	**8w**
	DOC-production (mg/L)	0.27 ± 0.00	0.15 ± 0.05	0.44 ± 0.05	1.13 ± 0.27	2.91 ± 0.71	5.00 ± 0.67
ESI+	**Assigned formulas**	44	67	223	340	355	247
	Average molecular mass	265.39 ± 86.07	292.12 ± 97.37	289.96 ± 91.65	278.61 ± 96.20	274.31 ± 99.52	325.60 ± 121.02
	Average H/C	1.52 ± 0.38	1.48 ± 0.46	1.60 ± 0.40	1.51 ± 0.40	1.29 ± 0.38	1.23 ± 0.38
	Average O/C	0.31 ± 0.17	0.35 ± 0.16	0.34 ± 0.17	0.27 ± 0.14	0.22 ± 0.13	0.36 ± 0.32
	Average AI	0.24 ± 0.23	0.26 ± 0.24	0.19 ± 0.22	0.24 ± 0.23	0.36 ± 0.21	0.35 ± 0.23
	Average DBE/C	0.33 ± 0.21	0.34 ± 0.23	0.29 ± 0.21	0.32 ± 0.21	0.43 ± 0.19	0.45 ± 0.18
ESI-	**Assigned formulas**	nd	nd	nd	3	306	313
	Average molecular mass	nd	nd	nd	517.62 ± 267.97	256.23 ± 111.59	349.93 ± 209.81
	Average H/C	nd	nd	nd	1.96 ± 0.05	1.07 ± 0.27	0.99 ± 0.24
	Average O/C	nd	nd	nd	0.31 ± 0.03	0.46 ± 0.19	0.32 ± 0.13
	Average AI	nd	nd	nd	0	0.41 ± 0.21	0.51 ± 0.14
	Average DBE/C	nd	nd	nd	0.07 ± 0.03	0.56 ± 0.14	0.59 ± 0.12

Part II. Toxicity Assessment of Photodegraded Plastic Particles (Polyethylene and Polycarbonate) on the Development of *Oryzias Melastigma*

Methods

1. Optimization of marine medaka (Oryzias melastigma) embryo husbandry

Our preliminary methods of embryo husbandry consisted of embryos being maintained in an incubator at 28°C that had a window to provide both light and dark exposure. This method resulted in below-average hatching rates for all control and treatment groups. To optimize hatching rates and embryo health, several preliminary studies were done to assess how lighting and aeration affected embryo hatching rates. Aeration did not appear to have an effect, but a light-dark cycle was essential in maintaining high hatching rates. Results showed that embryos hatched around the expected time of 7-10 days and had the greatest hatching rates while being cultivated in an incubator at 28ºC under a 12:12 light-dark cycle.

2. Preparation of marine medaka (Oryzias melastigma) embryos and treatment groups

Pairs of adult marine medaka are kept in 2.5-gallon breeding tanks with approximately 15 males and 15 females and are monitored daily for embryos. Tanks are kept at a salinity of 26-28 ppt, and water changes are performed every two weeks. Collected embryos are rinsed and cultured in glass Petri dishes with filtered artificial seawater and drops of methylene blue. Embryos are examined under a microscope to determine which embryos are 24 hours post-fertilization, using published standards of marine medaka development (Murata et al., 2019). Embryos 24 hours post-fertilization are maintained in an incubator at 28ºC under a 12:12 light-dark cycle, and water changes are performed twice a week.

2. Experimental Procedure and Observation of Embryos

Five types of plastic nurdles (PE, PP, PS, PET, and PC) were photodegraded in artificial seawater using a solar simulator for 8 weeks. The resulting leachate solution was diluted using artificial seawater to culture the embryos. To ensure embryos received the proper hatching signals and were raised in an environment resembling natural conditions, the artificial seawater used in the control treatment and to dilute the leachate solutions was prepared by combining 1 part filtered seawater from the adult breeding tanks and 1 part freshly made artificial seawater (28 ppt). To determine which polymers to study in-depth, preliminary exposures were performed on groups of 15 embryos for 14 days, and hatching (Fig. 1) and mortality rates were recorded. PC, PE, PET, and PS showed promising preliminary results and were chosen to study in-depth based on their effects on hatching, mortality, and deformity rates.

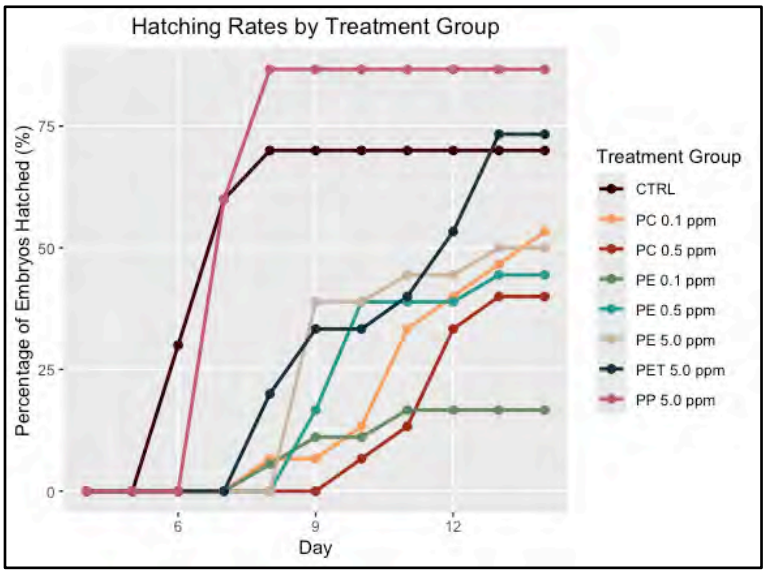

Figure 1: Hatching rates of medaka embryos exposed to PC (0.1, 0.5 ppm), PE (0.1, 0.5, 5.0 ppm), PET (5.0 ppm), PP (5.0 ppm), and a control.

3. Histological Staining and Analysis of Juveniles

Approximately 10 juvenile marine medaka were collected from each experimental tank and fixed in paraformaldehyde for histological examinations. Samples were embedded in paraffin wax, and horizontal 4-µm sections were cut using a rotary microtome (Leica RM2125 RTS). Sections were mounted onto glass slides (VWR® Superfrost Plus) and were deparaffinized and rehydrated before being stained with hemotoxin and eosin (H&E). Coverslips were mounted over the sections using Permount (Fisher Scientific) and observed under a compound microscope. Photos of the target organs, including the liver, gills, brain, and intestine, were taken to compare treatment and control samples.

Results

1. Preliminary PET treatment showed delayed hatching times and hatching deformities

No significant mortality was observed in the PET 5.0 ppm 4-week photodegraded leachate treatment group. Embryos in the PET treatment group showed delayed hatching times compared to the control. While all embryos in the control group hatched from days 7-10, embryos in the PET treatment hatched from days 9-14 (Fig. 1). Additionally, 20% of the embryos in the PET group showed a hatching deformity that resulted in inhibited locomotion. Deformities included spinal curvature and a failure to hatch completely, with the head partially encased within the egg membrane (Fig. 2). These results suggest that the effects of photodegraded PET may be worth investigating.

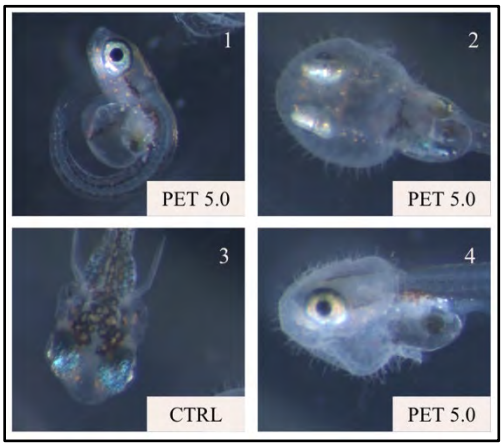

Figure 2: Morphology of medaka embryos exposed to PET (5.0 ppm). Deformities consisted of curved spines (1), and a failure to hatch completely (2, 4).

2. Preliminary PP treatment showed no significant mortalities or deformities

No significant mortality or deformities were observed in the PP preliminary study. Embryos hatched from days 7-9, which was comparable to the control group (Fig.1). 87% of embryos exposed to 5.0

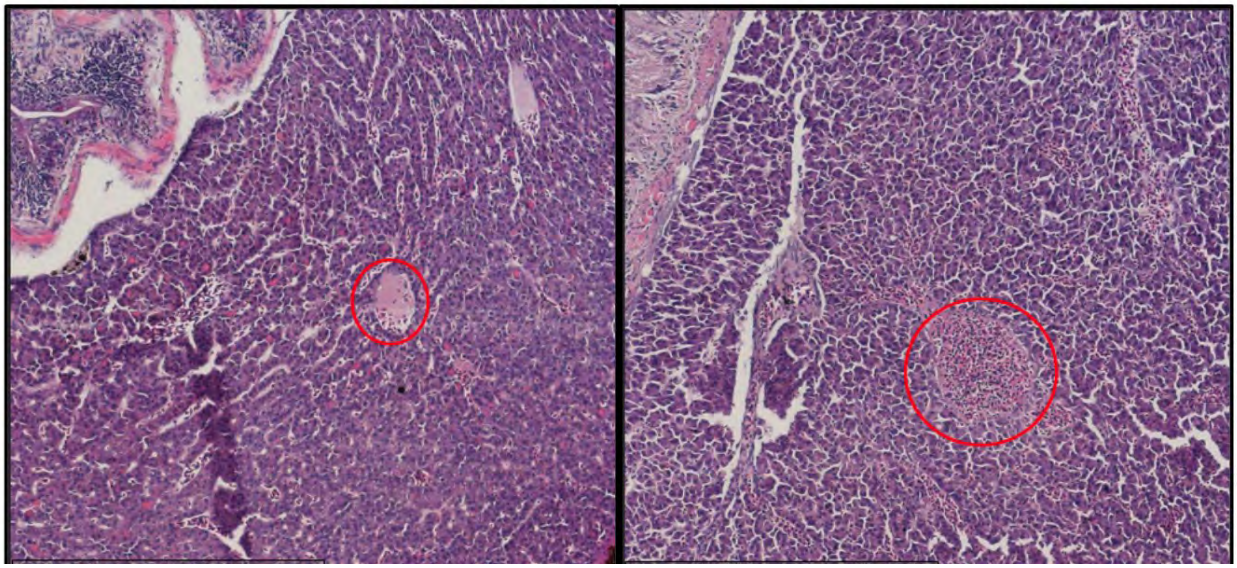

Figure 3: H&E staining of the liver of 3-month-old juvenile medaka exposed to PE (0.5). The red circle indicates an area of potential interest.

ppm PP leachate hatched around the same time, indicating that PP had little to no effect on the hatching rates or mortality of the embryos. Due to its similarities with the control group, PP is potentially not a good candidate for further investigation.

3. H&E staining of juvenile medaka shows differences in liver

Imaging of the liver in juvenile medaka exposed to PC and PE has shown potential evidence of venous congestion within the liver of medaka exposed to PE (Fig. 3). Further imaging and analysis need to be done to determine the frequency of this occurrence, and whether medaka exposed to PC experienced a similar effect. Additionally, more in-depth imaging and analysis will be done for the brain, kidneys, and gills to determine if any significant morphological changes occurred.

Experimental plan for next steps

1. Full-scale developmental studies of PC, PE, PET, and PS

To assess the early development of *O. melastigma*, developmental experiments will be run with the PS, PE, PC, and PET leachates. Embryos 24 hours post-fertilization will be randomly separated into the different treatment and control groups, with 20 embryos in each group. Embryo development will be monitored daily for a total of 14 days, and the stage of each embryo, as well as its mortality and hatching status, will be recorded. Throughout each study, the hatching rate, mortality rate, and body size will be measured, and any observed deformities before and after hatching will be noted and photographed.

Additionally, the heartbeat rate will be measured on days 4, 6, 8, and 10 by randomly selecting 5 embryos from each group and counting the number of heartbeats observed in 20 seconds under a compound microscope (Huang et al., 2011). Body length will be measured on day 14 by anesthetizing the hatched larvae using ice water and photographing them under a microscope. Measurements will be calculated using ImageJ.

2. Collection of embryos exposed to PC, PET, and PS for qPCR

To collect embryos for qPCR analysis, embryos 24 hours post-fertilization will be randomly divided into control and treatment groups and will be monitored for a total of 14 days. Beginning on day 7, embryos (n= 5) from each control and treatment group will be removed daily and prepared for qPCR. Target genes will include those involved in oxidative stress responses, the immune system, inflammatory pathways, and heart-related stress genes.

3. Toxicity assessment of marine medaka embryos and juveniles

To assess gene expression in marine medaka larvae and juveniles exposed to PC and PE leachate, qPCRs will be performed on collected embryos and juveniles. We will use several genetic markers that evaluate the stress levels of the marine medaka and have begun preparing our juvenile fish samples for genetic analysis, as well as embryos that have been exposed to PE.

References

Huang, Q., C. Fang, X. Wu, J. Fan, and S. Dong. 2011. Perfluorooctane sulfonate impairs the cardiac development of a marine medaka (Oryzias melastigma). Aquatic Toxicology 105:71–77.

Murata, K., Kinoshita, M., Naruse, K., Tanaka, M., & Kamei, Y. (Eds.). 2019. Medaka: Biology, Management, and Experimental Protocols, Volume 2. John Wiley & Sons.